JOURNAL OF GEOPHYSICAL RESEARCH, VOL. 103, NO. B4, PAGES 7431–7441, APRIL 10, 1998

Chemical- and Clapeyron-induced buoyancy at the 660 km discontinuity

Donald J. Weidner and Yanbin Wang[1]

Center for High Pressure Research and Department of Geosciences, State University of New York at Stony Brook

Abstract. The impact of phase equilibria and equation of state measurements on defining the buoyancy associated with the 660 km discontinuity is examined. Aluminum has a striking effect on the sequence of phase transitions expected at 660 km. With a pyrolite chemistry the sign of the phase transition contribution to buoyancy depends on temperature, with convection-assisting forces being victorious in hotter regions. Lower Al and/or temperature result in the perovskite-forming transformation resisting convection but with a much reduced magnitude compared with a pure olivine mantle. Density considerations suggest that there is no positive evidence for chemical-induced buoyancy across the 660 km discontinuity. The surface processing which forms a basaltic crust will cause a density contrast that assists convection in the transition zone but resists convection through the expanded garnet stability field of mid-ocean ridge basalt. The detailed seismic character of the 660 km depth region and its lateral variations hold the key to defining the location of the mantle state relative to the parameter space defined by Al and temperature in this study.

1. Introduction

The degree to which the 660 km discontinuity introduces either a barrier or a boost to whole-mantle convection depends on the buoyancy attributable to chemical and phase changes that are occurring across this depth [*Christensen*, 1991]. Chemically induced density changes of a few percent can entirely stop convection through the chemical boundary. Large negative Clapeyron slopes associated with density increases will force convection to become episodic [*Honda and Balachandar*, 1993; *Tackley et al.*, 1993]. Laboratory studies are now available that address these issues. In the past 5 years, equation of state studies using synchrotron X ray sources to measure density at high pressure and temperature in both the diamond anvil cells and in multi-anvil devices have matured [*Fei et al.*, 1992; *Wang et al.*, 1998a]. Phase equilibria studies have quantified phase transformations in simple chemical systems as well as complicated systems at the extreme pressures and temperatures of the 660 km discontinuity using multi-anvil devices. In this paper we explore the implications of these data on the buoyancy issues related to the 660 km discontinuity.

2. Phase Transformation Effects on Buoyancy

Buoyancy force per unit area is the product of $g \times \delta$, where g is the local gravitational acceleration and δ is excess mass per unit area. The value of δ is given by

$$\delta = \int (\Delta\rho)\, dz \qquad (1)$$

where $\Delta\rho$ is the excess density generated by the elevation or depression of the phase transition and the integration is over depth z. For a multicomponent system this becomes

$$\delta = -\sum v_i(\Delta\rho_i)(\partial z/\partial P)(\partial P/\partial T)_i \Delta T \qquad (2)$$

where v_i is the volume percent of the ith phase, $\Delta\rho_i$ is the density increase associated with the transition, $\partial z/\partial P$ is the factor converting depth to pressure, $\partial P/\partial T$ is the Clapeyron slope of the phase boundary, and ΔT is the excess temperature associated with the density anomaly. A negative value of $\delta/\Delta T$ will enhance convection, while a positive value will impede it.

The sign of the Clapeyron slope for the transition from spinel to perovskite and magnesiowustite is generally considered to be negative. *Navrotsky* [1980] provided thermodynamic reasons for such a negative slope, while *Ito and Yamada* [1982] and *Ito and Takahashi* [1989] confirmed this possibility experimentally. Calorimetric data by *Ito et al.* [1990] and more recently *Akaogi and Ito* [1993a, b], combined with phase equilibria observations, serve to estimate the P-T Clapeyron slope of the phase boundary separating these two fields as about −3 MPa/K. Since this transition involves a density increase of ~6%, it provides a buoyancy force that opposes convection. However, even in a pyrolite mantle, spinel will constitute <60% of the volume at this depth. The remainder of the material includes a majoritic-enriched garnet along with a Ca-bearing perovskite. The garnet (~30% in volume) will also undergo a transition to perovskite in the 660 km region with a density increase about twice as large as that for spinel, while the Ca-perovskite will already be in its stable lower mantle phase.

In contrast to the olivine component the pyroxene-garnet system has positive Clapeyron slopes for the perovskite-forming phase transition. The results of *Yusa et al.* [1993], based on thermochemical and phase equilibria data, suggest a slope for the garnet-to-perovskite transition of ~5 MPa/K for a partially disordered tetragonal garnet. Figure 1 illustrates the phase boundaries for the $MgSiO_3$ taken from *Gasparik* [1996]. Indeed, both the garnet-to-perovskite and the garnet-to-ilmenite transformations have positive slopes, while the ilmen-

[1]Now at Consortium for Advanced Radiation Sources, University of Chicago, Chicago, Illinois.

Paper number 97JB03511.
0148-0227/98/97JB-03511$09.00

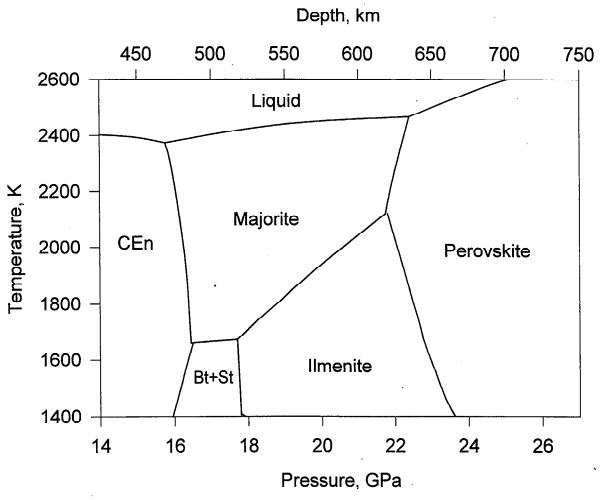

Figure 1. Phase diagram of $MgSiO_3$. Diagram modified after *Gasparik* [1996].

ite-to-perovskite has a negative slope. This system will provide a buoyancy force opposite to that of the spinel breakdown to perovskite and magnesiowustite at about the same depth.

In an Al free system the above parameters imply that $\delta/\Delta T$ will be negative for a 2:1 volume ratio of spinel and garnet transforming to the perovskite plus magnesiowustite assemblage. This will occur whether the garnet goes directly to perovskite or goes through the ilmenite phase, considering the relative slopes and density changes of all of the phases. Thus the phase transitions will enhance convection in this system as the net effect of the garnet transformation is greater than that of the spinel transformation. The velocity profile in such a system will have two or three closely spaced discontinuities caused by spinel-to-perovskite plus magnesiowustite and garnet-to- (possibly) ilmenite-to-perovskite transitions.

2.1. Role of Al on 660 km Phase Transitions

Adding Al to the system complicates the region, first, by broadening the depth range of the garnet-to-perovskite transition and, second, by linking the perovskite-producing reactions between the olivine and pyroxene normative portions. In this case the sign, the magnitude, and the shape of the buoyancy profile vary with Al content and ambient temperature.

In order to quantitatively calculate the buoyancy contributions of phase transformations, we need to determine the chemistry and volume percents of all phases that are present at pressures and temperatures in the 660 km region for model chemical compositions. Then, with appropriate equations of state for the different phases, the density and acoustic velocities can be defined and the effects of temperature variations inferred. Aluminum is very significant in defining phase fields of the system in this region. In this study, we use the CaO-MgO-Al_2O_3-SiO_2 (CMAS) system reported by *Gasparik* [1996] (see Figure 2) as a template for defining the evolution of the system through perovskite formation. The stability field of garnet for different pyrope contents is indicated by the thin solid lines in Figure 2. The expansion of the garnet field in pressure and temperature with increasing pyrope content indicates the degree to which Al stabilizes the garnet structure. The pyrope content indicated by these lines further represents the composition of the garnet phase that is in equilibrium with other pyroxene normative phases, be they pyroxene, ilmenite, or perovskite. In our calculations the olivine normative component is considered to be in either the spinel (Sp) structure or present as perovskite and magnesiowustite (Pv + Mw). The lower pressure wadsleyite field (beta phase), which is present in this P-T region in the iron free system of *Gasparik* [1996], is not included here as it will only occur at depths shallower than 540 km or so for pyrolite-like compositions. Figure 2 yields a Clapeyron slope of the spinel-to-perovskite plus magnesiowustite transition of −2 MPa/K and of the garnet-to-perovskite transition of +2.5 MPa/K, values slightly lower than suggested above but well within the range of uncertainty.

Predicting the effect of aluminum on the phase equilibria also requires knowledge of the Al content of the other phases that are in equilibrium with garnet. *Gasparik* [1990] reports that the Al content in spinel and ilmenite is negligible for these systems; however, perovskite does contain a significant amount of Al [e.g., *Irifune*, 1994]. Recently, *Irifune et al.* [1996] reported important new constraints on the pyrope-perovskite phase diagram at 1800 K. There is a relatively wide two-phase region of coexisting garnet and perovskite controlled by the Al content of the system. This can give rise to a gradient in seismic velocities in the vicinity of the 660 km discontinuity, superimposed on a discontinuity caused by the breakdown of spinel. We have adopted the results indicating the Al content in perovskite that is in equilibrium with garnet with some modifications since the

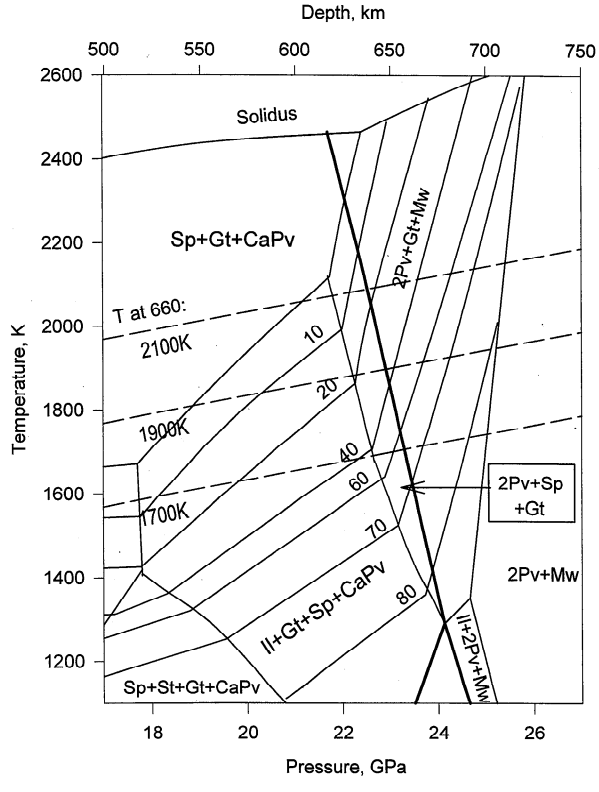

Figure 2. Phase diagram of the CMAS system (CaO-MgO-Al_2O_3-SiO_2) modified after *Gasparik* [1996]: Gt, garnet; Sp, spinel or ringwoodite phase; CaPv, $CaSiO_3$ perovskite phase; Pv, $MgSiO_3$ perovskite phase; Mw, magnesiowustite; St, stishovite; Il, $MgSiO_3$ in the ilmenite phase. Thick solid curves indicate the phase boundaries of the olivine normative system. The numbers on the thin solid curves indicate the pyrope content of the garnet in equilibrium with the other phases. Dashed curves indicate possible geotherms with labels that indicate the temperature at 660 km depth.

Table 1. Thermoelastic Parameters of Major Minerals for the Mantle

	(Mg,Fe)O Periclase	$X_3Y_2Si_3O_{12}$ Garnet*	$CaSiO_3$ Perovskite	(Mg,Fe)SiO_3 Perovskite	(Mg,Fe)$_2SiO_4$ Spinel	(Mg,Fe)SiO_3 Ilmenite
V_0, cm^3/mol	11.25(1)	113.985(5)	27.453(12)	24.46(14)	39.581(19, 20)	182.588(23)
$\partial \ln V/\partial$Fe	0.089(1)	0.023(6, 7)	···	0.042(15)	0.066(20)	0.025(24)
$\partial \ln V/\partial Ca$	···	0.141(7, 8)	···	···	···	···
$\partial \ln V/\partial Al$	···	−0.007(7)	···	···	···	···
K_{T0}, GPa	157(2)	160(5)	232(12)	261(16, 17)	184(20, 21)	210(25)
$(\partial K_{T0}/\partial P)_T$	4.0(2)	5.0(5, 9)	4.8(12)	4.0(17)	5.0(22)	4.0†
$(\partial K_T/\partial T)_P$, GPa K^{-1}	−0.027(2)	−0.021(5)	−0.033(12, 13)	−0.023(14)	−0.028(19)	−0.023†
$\alpha_0 = a + bT - c\,T^{-2}$						
a, 10^{-5} K^{-1}	3.84(2)	2.5(5)	3.0(12, 13)	1.64(14)	1.87(19)	2.27(26)
b, 10^{-8} K^{-2}	0.94(2)	0.9(5)	0.0(12)	0.86(14)	0.42(19)	1.2(26)
c, K	0.74(2)	0.0(5)	0.0(12)	0.0(14)	0.65(19)	0.0(26)
μ_0, GPa	130(3)	90(10)	175†	175(16)	119(21)	132(25)
$(\partial \mu_0/\partial P)_T$	2(3)	2.0(9)	1.8†	1.8†	1.5(22)	1.6†
$\partial \mu/\partial T$, GPa K^{-1}	−0.017(3)	−0.014†	−0.014†	−0.014†	−0.014†	−0.014†
γ_0	1.5(4)	1.2(11)	1.7(13)	1.4(14)	1.5(23)	1.5†
q	1.0†	1.0†	1.0†	1.0†	1.0†	1.0†
θ_D, K	500(4)	800(9)	1100†	1030(18)	900(22)	950(25)

Numbers in parentheses refer to the following sources: 1, *Hazen and Jeanloz* [1984]; 2, *Fei et al.* [1992]; 3, *Sumino and Anderson* [1984]; 4, *Suzuki* [1975]; 5, *Wang et al.* [1998b]; 6, *Matsubara et al.* [1990]; 7, *Ita and Stixrude* [1992]; 8, *Hazen et al.* [1994]; 9, *Rigden et al.* [1994]; 10, *Pacalo and Weidner* [1997]; 11, *Isaak et al.* [1992]; 12, *Wang et al.* [1996]; 13, *Wang and Weidner* [1994]; 14, *Wang et al.* [1994]; 15, *Parise et al.* [1990]; 16, *Yeganeh-Haeri et al.* [1989] and *Yeganeh-Haeri* [1994]; 17, *Knittle and Jeanloz* [1987]; 18, *Akaogi and Ito* [1993a, b]; 19, *Meng et al.* [1993, 1994]; 20, *Hazen et al.* [1993]; 21, *Weidner et al.* [1984]; 22, *Rigden et al.* [1991]; 23, *Ito and Matsui* [1978]; 24, *Duffy and Anderson* [1989]; 25, *Weidner and Ito* [1985]; 26, *Ashida et al.* [1988], *Ringwood* [1982], *Irifune and Ringwood* [1993], and *Ito and Katsura* [1989].

*Garnet V_0 is referenced for end-member majorite $MgSiO_3$, and its Fe dependence is an average of the $MgSiO_3$-(Mg,Fe)SiO_3 series and pyrope-almandine series (5 and 6 in the preceding list). Similarly, the Ca dependence is an average of the $MgSiO_3$-(Mg,Ca)SiO_3 series and pyrope-grossular series (7 and 6 in the preceding list).

†Assumed value.

absolute pressures inferred for the phase transitions differ by ~2 GPa from those of *Gasparik* [1996].

It is also important to model the aluminum content in garnet that is in equilibrium with spinel and magnesiowustite. Few data are available for this system. We assume that the pyrope content of the garnet that is in equilibrium with spinel, perovskite, and magnesiowustite on the univariant boundary indicating the breakdown of spinel remains constant at lower pressures. Thus, when spinel transforms to perovskite and magnesiowustite, the garnet composition does not change. We have explored a wide range of assumptions such as allowing pyrope to coexist with spinel. The effect on buoyancy is minor; however, the effect on acoustic velocity profile can be quite large.

In contrast to aluminum, iron-magnesium partitioning does not appreciably affect the phase boundaries in this region. *Ito and Takahashi* [1989] reported that the spinel-to-perovskite plus magnesiowustite and the ilmenite-to-perovskite reactions are virtually independent of the iron content. The effect of iron on the garnet stability field, however, is not well defined. The general topology of the phase diagram is probably correct, but the aluminum partitioning may well change with the addition of iron. Thus we expect our calculations to be representative of possible Earth models, with some uncertainty of the chemical variables that will produce such models.

To calculate density and elastic moduli at mantle pressure and temperature, we used the equation of state parameters for the relevant phases given in Table 1. The parameters are for the high-temperature Birch-Murnaghan equation of state given by

$$P = \tfrac{3}{2}K_0[(V_0/V)^{7/3} - (V_0/V)^{5/3}][1 + \tfrac{3}{4}(K_0' - 4)((V_0/V)^{2/3} - 1)] \quad (3)$$

where the zero subscript indicates the parameter at high temperature and room pressure. All parameters in Table 1 are referenced to room pressure and temperature.

Ito and Takahashi [1989] reported that iron partitions preferentially into the magnesiowustite phase rather than the coexisting perovskite. More recently, *Wood and Rubie* [1996] demonstrated that the magnesiowustite-perovskite iron partitioning is approximately equal in the presence of aluminum. However, iron-magnesium partitioning does not have a major effect on density or elastic properties in this system. The effect of iron on volume is small and similar between phases. Thus the total system volume is insensitive to where the iron resides. Iron affects the system density because of its higher weight, and it does not matter which phase is the iron reservoir. Similarly, bulk moduli are very insensitive to iron.

The effects of the iron oxidation state are not included in these calculations. *McCammon* [1997] argued that the lower mantle iron may be in mixed valance, and we have not explicitly accounted for any effect on volume of the oxidation state here. Iron generally causes the shear modulus to decrease, but the magnitude of this effect is poorly defined for these phases. Thus, in our calculations and without loss of accuracy of predicted property we assume that the Fe/Mg ratio is the same for all phases. We then make a correction to the zero pressure volume to reflect the iron content. All other parameters are taken to be independent of the Fe/Mg ratio. As a result, the room pressure shear modulus is probably overestimated. However, the pressure and temperature derivatives of this quantity are also estimated with comparable uncertainties.

Aluminum incorporation in most phases will occur by two Al cations replacing one Mg and Si pair. The effect of this substitution on physical properties is generally small. Table 2 summarizes physical properties for pyrope and majorite garnet and

Table 2. Effect of Al on Properties of Phases

	$MgSiO_3$ Ilmenite (1)	Al_2O_3 Corundum (2)	$MgSiO_3$ Majorite (3)	$Mg_3Al_2Si_3O_{12}$ Pyrope (4)
Property	P_0	P'	P_0	P'
V, cm^3	26.349	−0.0294	113.988	−0.0287
K_S, GPa	210.	0.205	162.8	0.201
μ, GPa	132.	0.235	90.	0.12
x	0.0	1.0	0.0	0.25

The effect of Al is expressed by $P = P_0\ (1 + x \times P')$, where P is a property of the material, P_0 is the property of the Al free material, and $x = 2Al/(2Al + Mg + Si)$, representing the subsitution of 2Al = Mg + Si. Numbers in parentheses refer to the following sources: 1, *Weidner and Ito* [1985]; 2, *Sumino and Anderson* [1984]; 3, *Pacalo and Weidner* [1997]; 4, *O'Neill et al.* [1991].

$MgSiO_3$-ilmenite and corundum, both examples of octahedral substitution of 2Al for Mg-Si. The parameter x represents the ratio of 2Al/(Mg+Si + 2Al). This value is zero for the magnesium-silicon rich end-member. It is 1 for corundum and 0.25 for pyrope. A physical parameter, P, can be expressed as

$$P = P_0(1 + x \times P') \tag{4}$$

where P' is determined for these two systems. For both volume and bulk modulus the values of P' are remarkably similar. The shear modulus is less consistent; however, the data are not particularly constraining. The garnets have a change in symmetry for tetragonal to cubic across this solid solution, and this change in symmetry complicates isolating the effects of the chemical change [*Sinogeikin et al.*, 1997]. For this study, we adapt the P' as defined by the ilmenite-corundum data. We apply the same coefficients to the garnet system as to the perovskite system, the only phases that are allowed to dissolve aluminum. In addition, we explicitly account for mass differences of the cations.

2.2. Buoyancy Resulting From 660 km Phase Transformations

The phase-transition-induced buoyancy is defined by calculating the stable phases, their compositions, and their densities as a function of depth along adiabatic gradients. *Ito and Katsura* [1989] estimated the temperature profile in the transition zone based on phase equilibrium data on the Mg_2SiO_4-Fe_2SiO_4 system and concluded that the thermal gradient below 530 km is ~0.35 K/km. *Brown and Shankland* [1981], however, gave a much higher temperature gradient (~0.68 K/km) to 771 km depth, beyond which the gradient is ~0.30 K/km in the lower mantle. The high gradient for the transition zone in the Brown and Shankland geotherm is most likely due to the high-velocity gradients given by the Preliminary Reference Earth Model (PREM) [*Dziewonski and Anderson*, 1981]. Here we adopt a uniform gradient of 0.35 K/km across 670 km depth with different foot temperatures. The phase-transition-induced buoyancy is then given by the integrated density difference for two temperatures (equation (1)) after correcting for the effects of thermal expansion on the density difference. Table 3 gives bulk compositions for a pyrolite model and a chondritic-based chemical model as defined by *McDonough and Sun* [1995]. As the Al content of *Ringwood*'s [1975] models tend to be slightly lower, we investigated the effect of lowering the Al content from that of *McDonough and Sun* [1995] to zero.

To illustrate the coupling of the chemical systems, we illustrate the phase relations with a few examples using Figure 2. Consider a pyrolite system that includes spinel and garnet along 1700, 1900, and 2100 K geotherms, respectively (the geotherm is referenced to the temperature at 660 km depth in this discussion). A pyrolite similar to that of *McDonough and Sun* [1995] of Table 3, but with 3 cation % Al, will have a 34% pyrope as the garnet phase in the lower transition zone. Five percent Al corresponds to a pyrope content of 53% in this region. As pressure increases along a 1900 K geotherm, this garnet along with spinel and Ca-perovskite remain stable until 650 km depth where the spinel breaks down to perovskite and magnesiowustite, while the garnet composition is just in equilibrium with perovskite. The volume percents of spinel and garnet are illustrated for this 3% Al system (Figure 3a) as well as the 5% Al system (Figure 3b). The spinel is aluminum free, but the perovskite in equilibrium with the garnet contains some aluminum. The large amount of $MgSiO_3$ contributed by the spinel to the perovskite demands that Al be added to the perovskite, and the only source of Al is garnet. Thus, at this point a significant amount of garnet transforms to perovskite until the Al/Si ratios of the perovskite and garnet reach their equilibrium values. Thus some garnet is forced to transform with the spinel at the spinel boundary. Along a 2100 K geotherm a 15% pyrope garnet can coexist with perovskite at the spinel-to-perovskite boundary. By our assumptions outlined above we define the maximum pyrope content in equilibrium with spinel at this temperature thereby to be equal to 15%, requiring some $(Mg,Fe)SiO_3$ from the spinel to dilute the Al in the garnet. This leaves (Mg,Fe)O as an additional phase. Thus, in this region the balance of spinel to garnet has changed to be more garnet rich as reflected in Figure 3. It may be possible to completely remove the spinel phase from this region as is seen for the 5% Al system at this temperature. Finally, consider the phase reactions along a 1700 K (Figure 2) geotherm. At 620 km the garnet begins to transform to ilmenite, enriching Al in the garnet until 645 km where ilmenite transforms to perovskite. The remaining garnet continues to transform as pressure increases. At 660 km, spinel transforms to perovskite and magnesiowustite, again forcing some garnet to accompany this transformation.

Model acoustic velocities and density are illustrated in Figure 4 for these compositions as a function of pressure along the various geotherms. In the case where garnet becomes more enriched because of the spinel breakdown (e.g., along the 2100

Table 3. Chemical Composition Models

Oxides	Pyrolite*	Cl*	MORB†	Harzburgite‡
		Weight Percent		
SiO_2	45.0	50.0	50.4	43.8
Al_2O_3	4.5	4.0	16.1	1.1
FeO	8.0	8.0	7.7	8.2
MgO	38.0	35.0	10.5	46.0
CaO	3.6	3.0	13.1	0.8
		Cation Percent		
Si^{4+}	38.4	42.8	47.8	36.0
Al^{3+}	4.5	4.0	18.0	1.1
Fe^{2+}	5.8	5.7	6.1	5.7
Mg^{2+}	48.1	44.7	14.8	56.4
Ca^{2+}	3.2	2.8	13.3	0.7

**McDonough and Sun* [1995].
†*Irifune and Ringwood* [1987b]. MORB, mid-ocean ridge basalt.
‡Based on pyrolite = .8 harzburgite + 0.2 MORB.

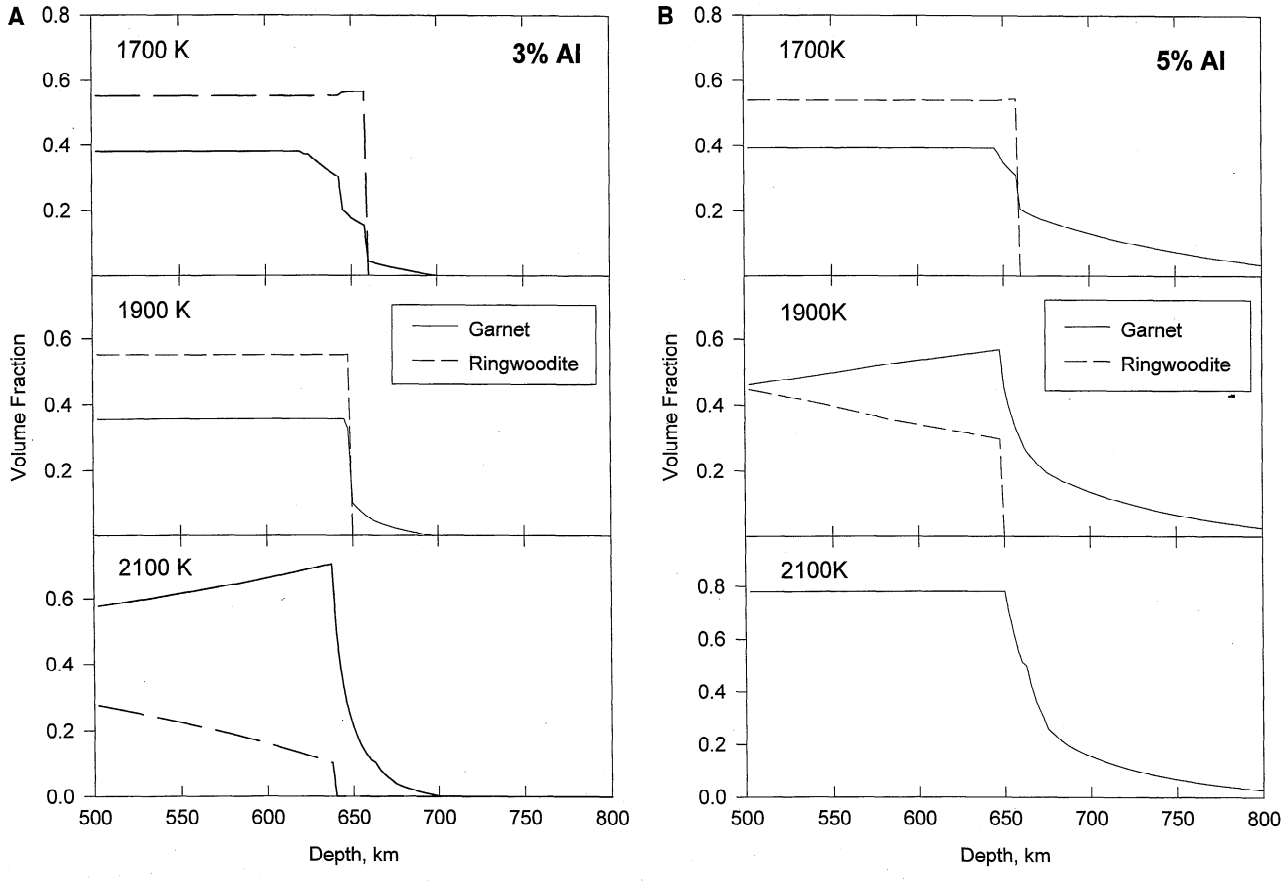

Figure 3. Calculated volume percent of garnet and ringwoodite as a function of depth along the three geotherms for a pyrolite-like composition: (a) a system with 3 cation % Al and (b) the results for 5% Al. Calculations are based on the phase diagrams described in Figures 1 and 2.

K geotherm), acoustic velocities decrease with increasing depth, because of garnet's low elastic moduli. The density profile is affected very little. For comparison, the properties of PREM are also illustrated in Figure 4. One note of caution is that the absolute values of the shear moduli are still poorly constrained by data. Thus the absolute values of the acoustic velocities are possibly in error. However, the shape of the discontinuities and gradients for the different cases is more robust.

Phase-transition-induced buoyancy is calculated as a function of temperature T by subtracting the densities calculated at $T - 100$ from that at T and integrating over depth after removing the effects of thermal expansion from the difference. The results for several compositions and ambient temperatures are illustrated in Figure 5 as a function of temperature T. Included are pyrolite compositions with different Al contents ranging from 0 to 5 cation %, pure olivine, and a Cl composition from Table 3. Also indicated in Figure 5 is the magnitude of the thermal expansion induced buoyancy for the range 500–800 km for a 100° temperature difference. The buoyancy effect due to larger values of ΔT can be obtained by integrating the appropriate buoyancy curve in temperature.

The pyrolite models with 4–5% Al demonstrate a large negative buoyancy at high temperature (assisting convection). Garnet is very stable and completely consumes the spinel phase. The transition is controlled by the garnet-to-perovskite reaction with its positive P-T slope. Pyrolite with 3% Al has a positive buoyancy throughout most of this temperature range but follows the same general pattern as the 4 and 5% systems. In general, the buoyancy increases (progressively resisting convection) as Al decreases from 5 to 2% where it is a maximum, almost equal to an entirely olivine mantle at some temperatures. This happens when the spinel breakdown forces most of the garnet to follow, thus forcing most of the material to be dominated by the negative Clapeyron slope of this transition. Further reducing the Al content decouples the two transitions and eventually leads to the mostly negative buoyancy of an Al free pyrolite.

The pyrolite model of *McDonough and Sun* [1995] is bounded by 4 and 5% Al. It is quite clear that pure olivine is not a good proxy for the expected effects of the 660 km discontinuity for these compositions and phase relations. The expected buoyancy of these more appropriate compositions remains less than half of a pure olivine mantle at any temperature and is large with the opposite sign at the higher, but realistic, 660 km depth temperatures.

The buoyancy for the chondritic model of Table 3 is also given in Figure 5. The effect of enriching Si relative to Mg has been to increase the amount of garnet in the system. Therefore almost all temperature and Al models have a negative buoyancy coefficient, thus assisting convection.

The location of the Earth in this chemical parameter space is still somewhat uncertain. If we accept the model of *McDonough and Sun* [1995], then the Earth may be close to the transition between the spinel-controlled region and the garnet-controlled region. Here the phase-transition-induced buoyancy

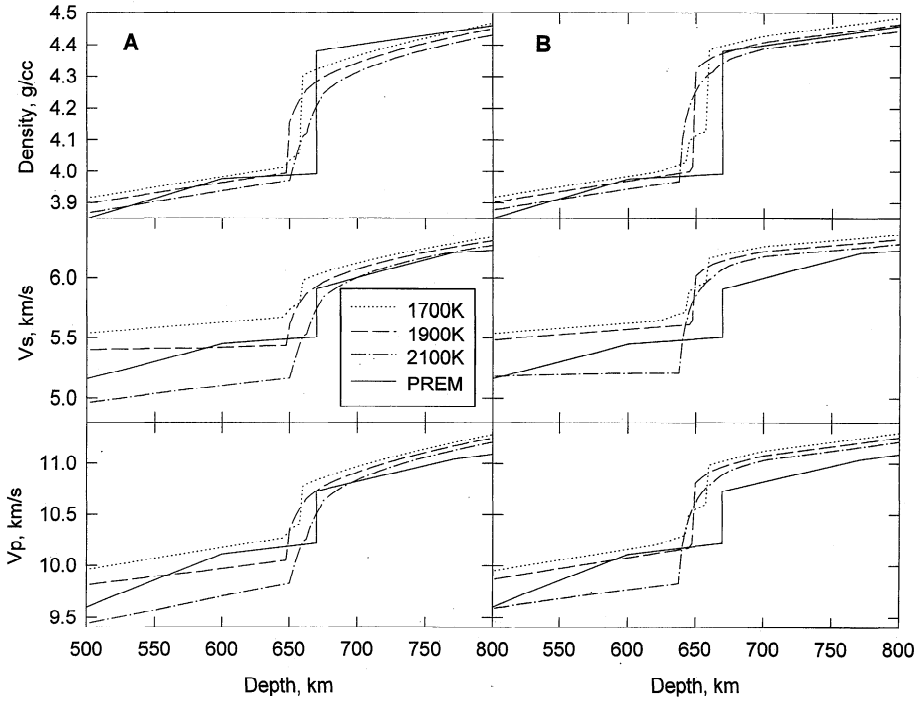

Figure 4. Calculated density and acoustic velocities for different geotherms for a pyrolite-like composition (a) for a model with 5% Al and (b) for 3% Al. The properties were calculated using the parameters of Table 1 and the phase diagrams described in Figures 1 and 2. The values for the preliminary reference Earth model (PREM) are included for reference.

is strongly temperature dependent, at low temperatures resisting convection, while at high temperatures assisting convection. Such a phenomenon could act as a thermostat. If the Earth were hot, then convection would proceed rapidly because of the garnet phase transitions until the spinel control began. Then convection would slow down.

3. Chemical-Induced Buoyancy

If the upper and lower mantle differ chemically in such a manner that the density of the lower mantle material is higher at lower mantle conditions, then convection is impeded. A few percent of such chemical-induced buoyancy are sufficient to force convection to be layered *Christensen* [1991]. With the equation of state parameters of Table 1 we calculate the density of the pyrolite model of Table 3 at lower mantle conditions and compare with PREM values [*Dziewonski and Anderson*, 1981]. Taking 1071 km depth as a reference depth that is far enough away from the 660 km discontinuity to be free of transition zone influences, yet shallow enough to be close to the P-T region where the equation of state parameters are valid, Figure 6 illustrates the trade-off between temperature and iron content as required to match the PREM density. We find that 2180 K (±150 K) is required for the model composition to match the observed density for an Fe/(Fe+Mg) value ratio of 0.107 (±0.01). Thus temperatures that differ from 2180 K at 1071 km depth must be compensated by a different iron content. However, this temperature falls well within the range of expected temperatures at this depth [e.g., see *Jeanloz and Knittle*, 1989]. The compatibility of composition and mantle temperature implies that the upper and lower mantles are neutrally buoyant.

Neutral buoyancy does not require chemical homogeneity. Figure 7 displays the chemical compositions in the MgO-FeO-SiO_2 ternary diagram that satisfy PREM density at 1071 km depth and 2180 K (thick line) and those that differ by ±0.5% (thin lines). The Fe/(Fe+Mg) ratio is the primary chemical variable that affects density. Figure 8 illustrates the density dependence on the Fe/(Fe+Mg) ratio at these conditions. The Ca-perovskite is 2% denser than the lower mantle at these conditions. Thus a few percent of this phase can be compensated by a slight decrease in Fe. Similarly, the magnesiowustite phase and the Mg-perovskite phases differ in density by less than 4% for the same Fe/Mg ratio at these conditions. Thus different Mg/Si compositions will yield the same density with a modest change in the bulk Fe/Mg ratio.

4. Processing-Induced Buoyancy

The above discussions are particularly relevant to upwelling regions or downwelling regions where there has been no chemical processing of the material and the P-T dependence of the phase relations and mineralogy of the ambient mantle are the same as those of the transitory material. Subduction zones must be considered differently because a basaltic layer has been physically separated from its residue, thereby creating chemical layering. The degree to which this chemical layering alters the bulk mineralogy or redefines pressures for phase transitions needs to be included in a description of buoyancy as advocated by *Ringwood* [1994]. In these models the processed region is considered to consist of layers of basalt, harzburgite, and pyrolite. A consistent chemistry for these regions is illustrated in Table 3, assuming pyrolite is equivalent to 0.2 mid-ocean ridge basalt (MORB) + 0.8 harzburgite. Phase relations of the basalt have been studied beginning with *Irifune and Ringwood* [1987a, b], who examined phase relations in these

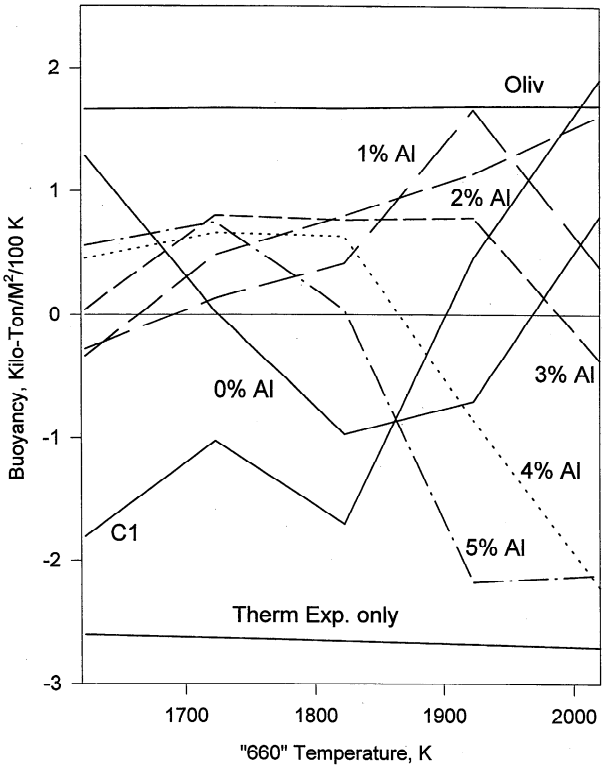

Figure 5. Excess mass per unit area due to phase transitions at 660 km depth as a function of temperature. The values represent the integrated density difference between two models which have a temperature difference of 100 K. The results are displayed for several pyrolite-like compositions but differing Al contents as indicated. Similar results are displayed for a Cl chondrite type model (Table 3) and pure olivine. The effect of integrating buoyancy resulting from just thermal expansion from 500 to 800 km depth is also indicated for reference. A negative value indicates that the buoyancy assists convection.

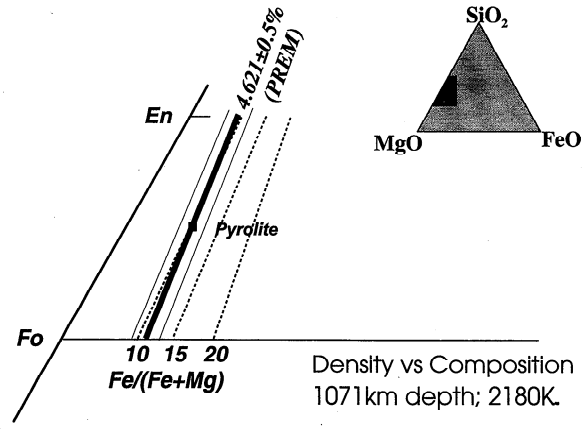

Figure 7. The effect of composition on density in the ternary diagram bounded by MgO, FeO, and SiO_2 (in offset). All compositions on the thick curve will have a density that agrees with PREM (4.621) at 1071 km depth and 2180 K. The parallel lines indicate compositions with a density 0.5% different than the PREM density; also dashed lines indicate constant Fe content. The small square indicates the composition of pyrolite.

assemblages between 24 and 28 GPa and 1500 and 1800 K and concluded that MORB is ~100 kg/m^3 (0.1 g/cm^3) denser than pyrolite up to 660 km and ~200 kg/m^3 less dense below that depth, while harzburgite is ~500 kg/m^3 less dense than pyrolite except in a narrow depth interval near 660 km.

The first item to consider is whether the mineralogy of a pyrolite equivalent package (PEP) containing MORB and harzburgite is buoyant relative to pyrolite at the same temperature in the transition zone and in the deep mantle. PEP differs from pyrolite principally by the oversaturation of silica in the MORB component and undersaturation in the harzburgite portion. Thus stishovite will be a significant phase in PEP,

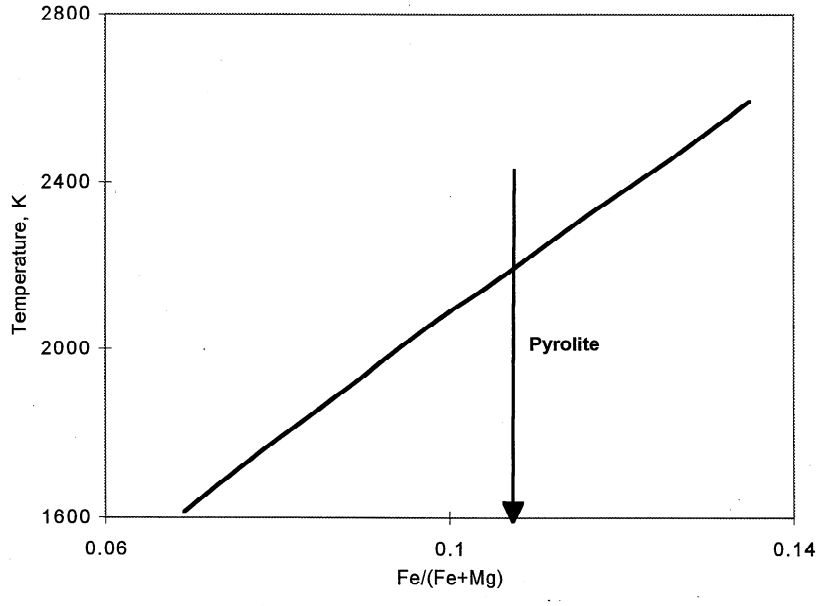

Figure 6. Trade-off between temperature and Fe content that satisfies the PREM density of 4.621 at 1071 km depth. Pyrolite composition corresponds to 2180 K at this depth.

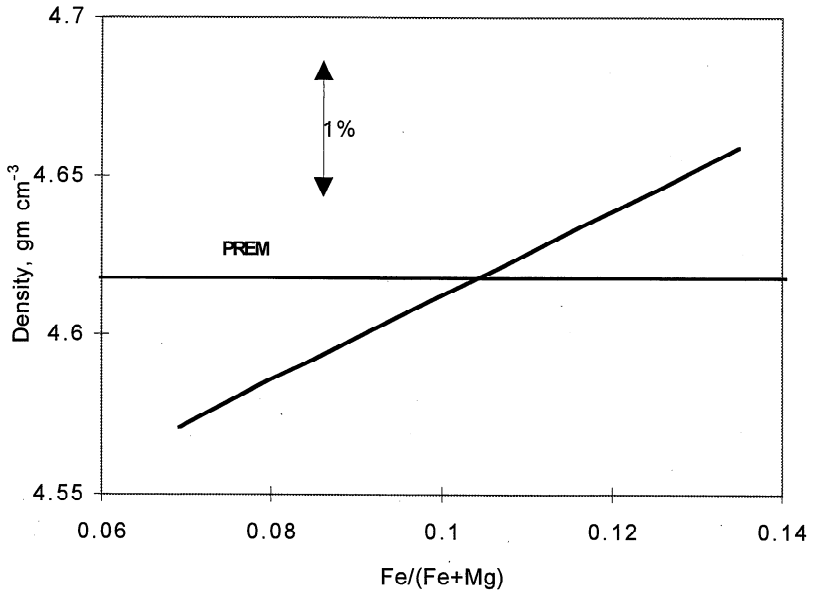

Figure 8. The effect of variations in Fe content on density at 1071 km depth and 2180 K.

while it is not present in pyrolite [see *Irifune*, 1993]. In the transition zone, ~12.5% of the total volume of pyrolite, which will be present in the garnet phase, will be present as a one-to-one molar mixture of gamma plus stishovite in PEP. Since the gamma plus stishovite is 5–7% denser in the transition zone than majorite, this will make the PEP system 0.6–0.8% denser than pyrolite at the same temperature throughout the transition zone. In addition, owing to the low Al content of the harzburgite, some of the garnet in the PEP system will transform to the 1% denser ilmenite phase in the 550–650 km depth range. Thus PEP will be between 0.6 and 1.0% denser than pyrolite throughout the transition zone owing to the chemical processing that occurred at the surface.

In the lower mantle, *Kesson et al.* [1994] has reported that basaltic compositions eventually transform to two perovskites, stishovite, and a Na/Al rich calcium ferrite phase. Since the composition of the Ca-ferrite phase contains about equal amounts of Si and (Mg+Fe), it does not alter the degree of silica oversaturation. Thus, in the lower mantle, ~5.8 vol % of pyrolite which is present in the Mg-perovskite phase will be present as stishovite plus magnesiowustite in PEP. In this case, however, the PEP assemblage is 3–5% less dense than that of pyrolite. The net effect is a reduction of PEP density by 0.17–0.3%. The Ca-ferrite phase is present in lower total abundance, and its effect is difficult to estimate owing to restricted knowledge of its properties. Thus we expect that PEP will be buoyant relative to pyrolite at the same temperature in the lower mantle after the perovskite-forming transformations have been completed in both systems [see *Kesson et al.*, 1997].

The second consideration concerns the effect of this processing on the depth of the perovskite-forming phase transitions. For harzburgite and pyrolite we find that the density difference is a complex function of mantle temperature and alumina content. To illustrate the results, Figures 9a and 9b show density difference between pyrolite and harzburgite at

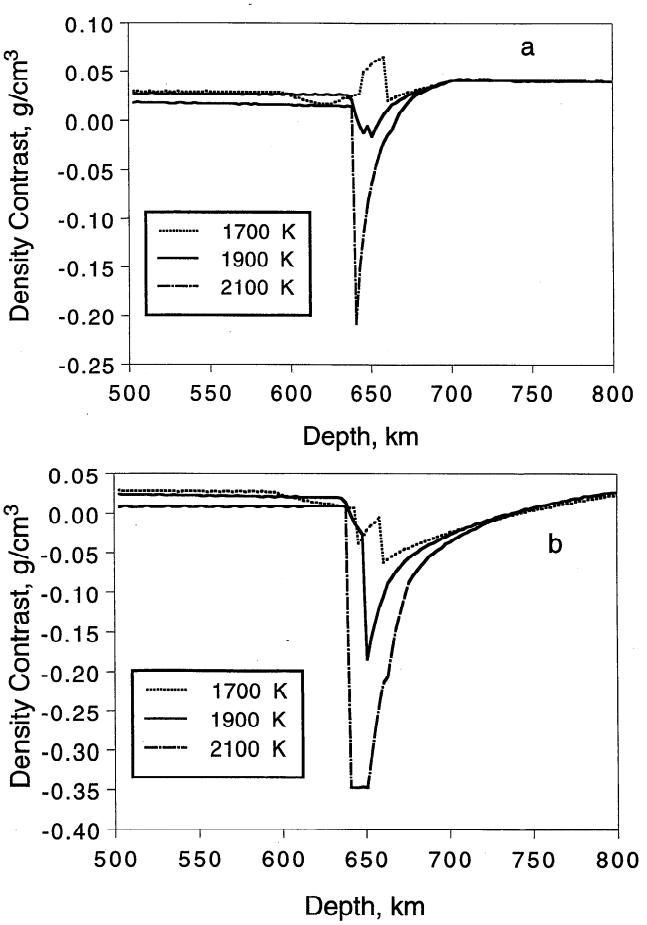

Figure 9. Density difference between pyrolite-like compositions and harzburgite (Table 3) as a function of depth for several geotherms. Both compositions are at the same temperature: (a) pyrolite with 3% Al and (b) a system with 5% Al.

the same temperature as a function of depth with an Al content in the pyrolite of 3 and 5 cation %, respectively. All models start with a density contrast ≤0.5% at ~500 km depth (pyrolite being denser than harzburgite), which is consistent with the results of *Irifune and Ringwood* [1993] and the above discussion (this low density of harzburgite is more than compensated by the MORB component of PEP). However, as the slab approaches the 660 km discontinuity, vastly different density contrasts can be obtained, depending on temperature and alumina content of the ambient mantle. In the coldest models with 3% Al, harzburgite undergoes the perovskite-forming transformation at a shallower depth than pyrolite with a positive density contrast in the region of the transformation. In the hottest model with 5% Al, harzburgite undergoes the transformation at the shallowest depth with a large, subduction-assisting, negative buoyancy relative to pyrolite. Note that in previous studies the olivine and pyroxene normative components were treated as independent in perovskite-forming reactions and the variety of features demonstrated here were not observed. Figure 10 illustrates the net buoyancy of harzburgite relative to various chemical models as integrated over the 500–800 km depth region as a function of temperature and composition. Thus even harzburgite will have an overall density greater than pyrolite (4.5% Al) for the higher-temperature models owing to the role of Al in the perovskite-forming transformations in the pyrolite.

The phase transformations in MORB, however, will most certainly resist convection. *Irifune and Ringwood* [1993] demonstrate that garnet persists to higher pressure in MORB than in pyrolite. *Kesson et al.* [1994] determined that the MORB composition eventually transforms to a perovskite assemblage and suggested that this would occur by ~900 km depth, leaving a 250 km depth region where the garnet of the MORB portion of the subducted slab is surrounded by a much denser perovskite system in the ambient mantle as well as the harzburgite. Other studies [*Faust and Knittle*, 1996; *O'Neill and Jeanloz*, 1994] suggest that the garnet phase may persist to as deep as 1200 km. The density difference between perovskite and garnet is sufficient to render the PEP system less dense at the same temperature throughout the zone where garnet persists in the MORB portion.

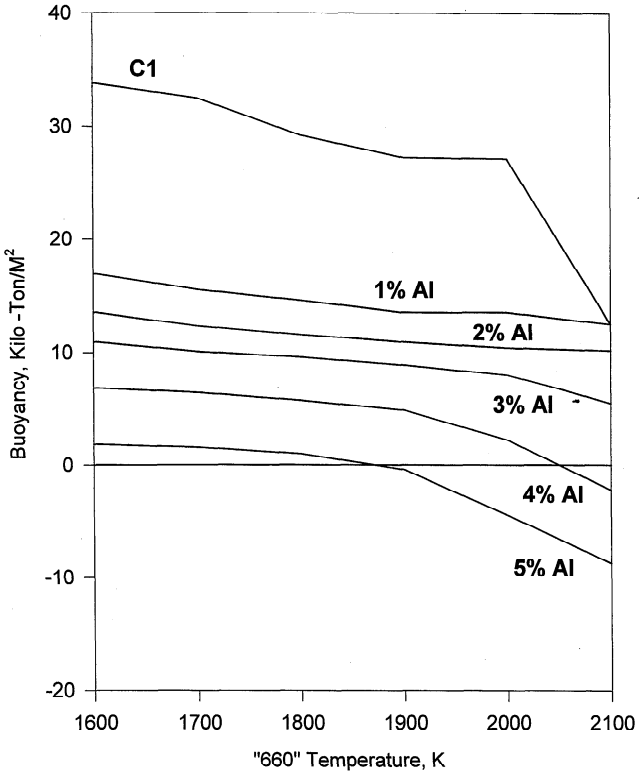

Figure 10. Integrated buoyancy of a harzburgite slab in a pyrolite media as a function of temperature while both are at the same temperature. Integration is along a geotherm from 500–800 km and referenced to the temperature at 660 km depth; the Al content is indicated on the curve, and Cl is for the chondrite of Table 3.

5. Conclusions

The phase relations at 660 km depth are quite complex. Al couples the olivine normative portion of the system to the pyroxene normative system. The perovskite-forming reactions have different Clapeyron slopes: positive for the garnet portion and negative for the spinel portion. One or the other of these two transitions will dominate the perovskite-forming reaction with the associated buoyancy implications. Within the current laboratory-defined parameter space and expected mantle temperatures, pyrolite appears to be at the crossroads between spinel dominance and garnet dominance. Thus a hotter mantle implies that the 660 km buoyancy will assist convection, while a colder mantle will encounter phase transitions that impede mantle convection.

It may be possible to identify where the Earth is actually located in this parameter space by careful analysis of 660 km seismic signatures. If the transition is spinel controlled, then we expect the discontinuity to be deeper in colder regions. Conversely, garnet control will deepen the discontinuity in hotter regions. The pyrolite model discussed here will see a nonlinear dependence of discontinuity depth on temperature. In Figure 4b, for 5% Al, the shallowest discontinuity corresponds to the intermediate temperature. Thus, in cold subduction zones the discontinuity would be expected to deepen, while in hot upwelling regions it would also deepen. The structure of the discontinuity differs at these different temperatures. In the lowest temperatures we can expect to see precursory velocity changes associated with the garnet transformation to ilmenite and ilmenite-to-perovskite reactions. In hotter regions the garnet-to-perovskite transition will add a broad steep velocity increase deeper than the 660 km discontinuity. If garnet dominates the 660 km transition, then we expect larger velocity increases than if spinel rules the transformation. Indeed, all of these features have been reported in different seismic models of the 660 km discontinuity. Coupling of the seismic information with the mineral modeling will give new insights concerning the actual buoyancy effects that are active in the Earth's mantle.

The density information suggests that there is no chemically induced buoyancy at the 660 km discontinuity. While this does not require the chemical composition to be identical above and below the 660 km discontinuity, it does imply that there is no convection impediment associated with any chemical change.

Processing of the mantle at the surface by separating basalt from pyrolite does have some buoyancy implications. The processed package will be denser than the surrounding pyrolite throughout the transition zone and less dense in the lower mantle. Furthermore, phase transitions in harzburgite will fol-

low much the same conclusions as for pyrolite, since these transitions are sensitive to the Al content and temperature of the ambient mantle. While MORB will ultimately undergo the densification phase transformations associated with perovskite formation, it will be retarded and represents a strong buoyant element, resisting convection to great depths.

Acknowledgments. The authors would like to thank T. Jordan, J. Gaherty, and P. Puster for stimulating discussion of this work. This research was supported by NSF through grant EAR9418689 and through CHiPR (grant EAR8920239). This is MPI publication 207. D.J.W. appreciates the University of Chicago, Department of Geophysical Sciences, for hosting his stay as a visiting faculty member during the time of this research.

References

Akaogi, M., and E. Ito, Heat capacity of $MgSiO_3$ perovskite, *Geophys. Res. Lett.*, *20*, 105–108, 1993a.

Akaogi, M., and E. Ito, Refinement of enthalpy measurement of $MgSiO_3$ perovskite and negative pressure-temperature slopes for perovskite-forming reactions, *Geophys. Res. Lett.*, *20*, 1839–1842, 1993b.

Ashida, T., S. Kume, E. Ito, and A. Navrotsky, $MgSiO_3$ ilmenite: Heat capacity, thermal expansion, and enthalpy of transformation, *Phys. Chem. Miner.*, *16*, 239–245, 1988.

Brown, J. M., and T. J. Shankland, Thermodynamic properties in the Earth as determined from seismic profiles, *Geophys. J. R. Astron. Soc.*, *66*, 579–596, 1981.

Christensen, U., The influence of phase transitions and chemical heterogeneity on the mantle convection, *Eclogae Geol. Helv.*, *84*, 317–326, 1991.

Duffy, T. S., and D. L. Anderson, Seismic velocities in mantle minerals and the mineralogy of the upper mantle, *J. Geophys. Res.*, *94*, 1895–1912, 1989.

Dziewonski, A. M., and D. L. Anderson, Preliminary reference Earth model, *Phys. Earth Planet. Inter.*, *25*, 297–356, 1981.

Faust, J., and E. Knittle, The stability and equation of state of majoritic garnet synthesized from natural basalt at mantle conditions, *Geophys. Res. Lett.*, *23*, 3377–3380, 1996.

Fei, Y., H. K. Mao, J. Shu, and J. Hu, P-V-T equation of state of magnesiowustite $(Mg_{0.6}Fe_{0.4})O$, *Phys. Chem. Miner.*, *18*, 416–422, 1992.

Gasparik, T., Phase relations in the transition zone, *J. Geophys. Res.*, *95*, 15,751–15,769, 1990.

Gasparik, T., Melting experiments on the enstatite-diopside join at 70-224 kbar, including the melting of diopside, *Contrib. Mineral. Petrol.*, *124*, 139–153, 1996.

Hazen, R. M., and R. Jeanloz, Wüstite $(Fe_{1-x}O)$: A review of its defect structure and physical properties, *Rev. Geophys.*, *22*, 37–46, 1984.

Hazen, R. M., R. T. Downs, L. W. Finger, and J. Ko, Crystal chemistry of ferromagnesian silicate spinels: Evidence for Mg-Si disorder, *Am. Mineral.*, *78*, 1320–1323, 1993.

Hazen, R. M., R. T. Downs, P. G. Conrad, L. W. Finger, and T. Gasparik, Comparative compressibilities of majorite-type garnets, *Phys. Chem. Miner.*, *21*, 344–349, 1994.

Honda, S., and D. R. S. Balachandar, Three-dimensional mantle dynamics with an endothermic phase transition, *Geophys. Res. Lett.*, *20*, 221–224, 1993.

Irifune, T., Phase transformations in the Earth's mantle and subducting slabs: Implications for their compositions, seismic velocity and density structures and dynamics, *Island Arc*, *2*, 55–71, 1993.

Irifune, T., Absence of an aluminous phase in the upper part of the Earth's lower mantle, *Nature*, *370*, 131–133, 1994.

Irifune, T., and A. E. Ringwood, Phase transformations in a harzburgite composition to 26 GPa: Implications for dynamical behavior of the subducting slab, *Earth Planet. Sci. Lett.*, *86*, 365–376, 1987a.

Irifune, T., and A. E. Ringwood, Phase transformations in primitive MORB and pyrolite compositions to 25 GPa and some geophysical implications, in *High-Pressure Research in Mineral Physics*, edited by M. H. Manghnani and Y. Syono, pp. 231–242, AGU, Washington, D. C., 1987b.

Irifune, T., and A. E. Ringwood, Phase transformations in subducted oceanic crust and buoyancy relationships at depths of 600–800 km in the mantle, *Earth Planet. Sci. Lett.*, *117*, 101–110, 1993.

Irifune, T., T. Koizumi, and J. Ando, An experimental study of the garnet-perovskite transformation in the system $MgSiO_3$-$Mg_3Al_2Si_3O_{12}$, *Phys. Earth Planet. Inter.*, *96*, 147–157, 1996.

Isaak, D. G., O. L. Anderson, and H. Oda, High-temperature thermal expansion and elasticity of calcium-rich garnets, *Phys. Chem. Miner.*, *19*, 106–120, 1992.

Ita, J., and L. Stixrude, Petrology, elasticity, and composition of the mantle transition zone, *J. Geophys. Res.*, *97*, 6849–6866, 1992.

Ito, E., and T. Katsura, A temperature profile of the mantle transition zone, *Geophys. Res. Lett.*, *16*, 425–428, 1989.

Ito, E., and Y. Matsui, Silicate ilmenites and the post spinel transformations, in *High-Pressure Research: Applications in Geophysics*, edited by M. H. Manghnani and S. Akimoto, pp. 193–206, Academic, San Diego, Calif., 1978.

Ito, E., and E. Takahashi, Post-spinel transformations in the system Mg_2SiO_4-Fe_2SiO_4 and some geophysical implications, *J. Geophys. Res.*, *94*, 10,637–10,646, 1989.

Ito, E., and H. Yamada, Stability relations of silicate spinels, ilmenites, and perovskites, in *High Pressure Research in Geophysics*, edited by S. Akimoto and M. Manghnani, pp. 405–419, Terra. Sci., Tokyo, 1982.

Ito, E., M. Akaogi, L. Topor, and A. Navrotsky, Negative pressure-temperature slopes for reactions forming $MgSiO_3$ perovskite from calorimetry, *Science*, *249*, 1275–1278, 1990.

Jeanloz, R., and E. Knittle, Density and composition of the lower mantle, *Philos. Trans. R. Soc. London, Ser. A*, *328*, 377–389, 1989.

Kesson, S. E., J. D. FitzGerald, and J. M. G. Shelley, Mineral chemistry and density of subducted basaltic crust at lower-mantle pressures, *Nature*, *372*, 767–769, 1994.

Kesson, S. E., J. D. FitzGerald, and J. M. G. Shelley, Phase chemistry and dynamics of a pyrolite lower mantle, paper presented at 9th Meeting, Eur. Union of Geosci., Strasbourg, France, 1997.

Knittle, E., and R. Jeanloz, Synthesis and equation of state of (Mg, Fe)SiO_3 perovskite to over 100 gigapascals, *Science*, *235*, 668–670, 1987.

Matsubara, R., H. Toraya, S. Tanaka, and H. Sawamoto, Precision lattice-parameter determination of $(Mg,Fe)SiO_3$ tetragonal garnets, *Science*, *247*, 697–699, 1990.

McCammon, C., Perovskite as a possible sink for ferric iron in the lower mantle, *Nature*, *387*, 694–696, 1997.

McDonough, W. F., and S.-S. Sun, The composition of the Earth, *Chem. Geol.*, *120*, 223–253, 1995.

Meng, Y., D. J. Weidner, G. D. Gwanmesia, R. C. Liebermann, M. T. Vaughan, Y. Wang, K. Leinenweber, R. E. Pacalo, A. Yeganch-Haeri, and Y. Zhao, In situ high P-T X ray diffraction studies on three polymorphs (α, β, γ) of Mg_2SiO_4, *J. Geophys. Res.*, *98*, 22,199–22,207, 1993.

Meng, Y., Y. Fei, D. J. Weidner, G. D. Gwanmesia, and J. Hu, Hydrostatic compression of γ-Mg_2SiO_4 to mantle pressures and 700 K: Thermal equation of state and related thermoelastic properties, *Phys. Chem. Miner.*, *21*, 407–412, 1994.

Navrotsky, A., Lower mantle phase transitions may generally have negative pressure-temperature slopes, *Geophys. Res. Lett.*, *7*, 709–711, 1980.

O'Neill, B., and R. Jeanloz, $MgSiO_3$-$FeSiO_3$-Al_2O_3 in the Earth's lower mantle: Perovskite and garnet at 1200 km depth, *J. Geophys. Res.*, *99*, 19,901–19,915, 1994.

O'Neill, B., J. D. Bass, G. R. Rossman, C. A. Geiger, and K. Langer, Elastic properties of pyrope, *Phys. Chem. Miner.*, *17*, 617–621, 1991.

Pacalo, R. E. G., and D. J. Weidner, Elasticity of majorite, $MgSiO_3$ tetragonal garnet, *Phys. Earth Planet. Inter.*, *99*, 145–154, 1997.

Parise, J. B., Y. Wang, A. Yeganeh-Haeri, D. E. Cox, and Y. Fei, Crystal structure and thermal expansion of $(Mg,Fe)SiO_3$ perovskite, *Geophys. Res. Lett.*, *17*, 2089–2092, 1990.

Rigden, S. M., G. D. Gwanmesia, J. D. FitzGerald, I. Jackson, and R. C. Liebermann, Spinel elasticity and seismic structure of the transition zone of the mantle, *Nature*, *354*, 143–145, 1991.

Rigden, S. M., G. D. Gwanmesia, and R. C. Liebermann, Elastic wave velocities of a pyrope-majorite garnet to 3 GPa, *Phys. Earth Planet. Inter.*, *86*, 35–44, 1994.

Ringwood, A. E., *Composition and Petrology of the Earth's Mantle*, McGraw-Hill, New York, 618 pp., 1975.

Ringwood, A. E., Phase transformations and differentiation in sub-

ducted lithosphere: Implications for mantle dynamics, basalt petrogenesis, and crustal evolution, *J. Geol.*, *90*, 611–643, 1982.

Ringwood, A. E., Role of the transition zone and 660 km discontinuity in the mantle dynamics, *Phys. Earth Planet. Inter.*, *86*, 5–24, 1994.

Sinogeikin, S., J. D. Bass, B. O'Neill, and T. Gasparik, Elasticity of tetragonal end-member majorite and solid solution in the system $Mg_4Si_4O_{12}$-$Mg_3Si_3O_{12}$, *Phys. Chem. Miner.*, *24*, 115–121, 1997.

Sumino, Y., and O. L. Anderson, Elastic constants of minerals, in *Handbook of Physical Properties of Rocks*, vol. 3, edited by R. S. Carmichael, pp. 39–137, CRC Press. Boca Raton, Fla., 1984.

Suzuki, I., Thermal expansion of periclase and olivine and their anharmonic properties, *J. Phys. Earth*, *23*, 145–159, 1975.

Tackley, P. J., D. J. Stevenson, G. A. Glatzmaier, and G. Schubert, Effects of an endothermic phase transition at 670 km depth in a spherical model of convection in the Earth's mantle, *Nature*, *361*, 699–703, 1993.

Wang, Y., and D. J. Weidner, Thermoelasticity of $CaSiO_3$ perovskite and implications for the lower mantle, *Geophys. Res. Lett.*, *21*, 895–898, 1994.

Wang, Y., D. J. Weidner, R. C. Liebermann, and Y. Zhao, P-V-T equation of state of $(Mg,Fe)SiO_3$ perovskite: Constraints on composition of the lower mantle, *Phys. Earth Planet. Inter.*, *83*, 13–40, 1994.

Wang, Y., D. J. Weidner, and Y. Meng, Advances in equation-of-state measurements in SAM-85, in *Properties of Earth and Planetary Materials at High Pressure and Temperature, Geophys. Monogr. Ser.*, vol. 101, edited by M. H. Manghnani and T. Yagi, pp. 365–372, AGU, Washington, D. C., 1998a.

Wang, Y., D. J. Weidner, J. Zhang, G. D. Gwanmesia, and R. C. Liebermann, Thermal equation of state of garnets along the pyrope-majorite join, *Phys. Earth Planet. Inter.*, in press, 1998b.

Wang, Y. B., D. J. Weidner, and F. Guyot, Thermal equation of state of $CaSiO_3$ perovskite, *J. Geophys. Res.*, *101*, 661–672, 1996.

Weidner, D. J., and E. Ito, Elasticity of $MgSiO_3$ in the ilmenite phase, *Phys. Earth Planet. Inter.*, *40*, 65–70, 1985.

Weidner, D. J., H. Sawamoto, S. Sasaki, and M. Kumazawa, Single-crystal elastic properties of the spinel phase of Mg_2SiO_4, *J. Geophys. Res.*, *89*, 7852–7860, 1984.

Wood, B. J., and D. C. Rubie, The effect of alumina on phase transformations at the 660 kilometer discontinuity from Fe-Mg partitioning effects, *Science*, *273*, 1522–1524, 1996.

Yeganeh-Haeri, A., Synthesis and re-investigation of the elastic properties of single-crystal magnesium silicate perovskite, *Phys. Earth Planet. Inter.*, *87*, 111–121, 1994.

Yeganeh-Haeri, A., D. J. Weidner, and E. Ito, Elasticity of $MgSiO_3$ in the perovskite structure, *Science*, *243*, 787–789, 1989.

Yusa, H., M. Akaogi, and E. Ito, Calorimetric study of $MgSiO_3$ garnet and pyroxene: Heat capacities, transition enthalpies, and equilibrium phase relations in $MgSiO_3$ at high pressures and temperatures, *J. Geophys. Res.*, *98*, 6453–6460, 1993.

Y. Wang, Consortium for Advanced Radiation Sources, University of Chicago, 5640 South Ellis Avenue, Chicago, IL 60637. (e-mail: wang@cars.uchicago.edu)

D. J. Weidner, Center for High Pressure Research, State University of New York at Stony Brook, Stony Brook, NY 11794-2100. (dweidner@sunysb.edu)

(Received June 3, 1997; revised October 14, 1997;
accepted November 24, 1997.)